

Topology of Disordered 3D Graphene Networks

Jacob W. Martin^{1,2,*}, Carla de Tomas,³ Irene Suarez-Martinez,³ Markus Kraft,^{1,2,4} and Nigel A. Marks³

¹*Department of Chemical Engineering and Biotechnology, University of Cambridge, West Site, Philippa Fawcett Drive, Cambridge CB3 0AS, United Kingdom*

²*Cambridge Centre for Advanced Research and Education in Singapore (CARES), CREATE Tower, 1 Create Way, Singapore 138602*

³*Department of Physics and Astronomy, Curtin University, Perth WA 6845, Australia*

⁴*School of Chemical and Biomedical Engineering, Nanyang Technological University, Singapore 637459*



(Received 25 February 2019; published 13 September 2019)

Disordered carbons comprise graphene fragments assembled into three-dimensional networks. It has long been debated whether these networks contain positive curvature, as seen in fullerenes, negative curvature, as proposed for the schwarzite structures, or zero curvature, as in ribbons. We present a mesh-based approach to analyze the topology of a set of nanoporous and glassy carbon models that accurately reproduce experimental properties. Although all three topological elements are present, negatively curved structures dominate. At the atomic level, analysis of local environments shows that sp - and sp^3 -bonded atoms are associated with line defects and screw dislocations that resolve topological complexities such as termination of free edges and stacking of low curvature regions into ribbons. These results provide insight into the synthesis of porous carbon materials, glassy carbon and the graphitizability of carbon materials.

DOI: [10.1103/PhysRevLett.123.116105](https://doi.org/10.1103/PhysRevLett.123.116105)

Determining the topology of disordered graphene networks is a long-standing problem in carbon science. In the 1940s, Rosalind Franklin observed stacked graphitic crystallites emerging during heat treatment of carbons. In isotropic (nongraphitizing) carbons these crystallites did not align and could not grow into large graphitic crystals, being restricted in their size and degree of stacking. Franklin proposed that crosslinks between the crystallites maintain their 3D connectivity and inhibited alignment [1]. In the 1960s, high resolution transmission electron microscopy (HRTEM) showed crosslinks between crystallites to be curved ribbon structures. Jenkins and Kawamura proposed a knotted ribbon model containing branches and forks [2]; using the language of differential geometry, we could describe such structures as locally Gauss flat, i.e., curvature $K \approx 0$, with only one nonzero principle axis of curvature [3]. However, this branched topology creates high porosity and large fractions of reactive edges, inconsistent with experiments [4].

The 1985 discovery of fullerenes provided new connectivity possibilities within graphene networks [5]. Harris, in 1997, was the first to suggest fullerene-like structures in isotropic carbons, evidenced from his electron micrographs of polygonalized structures in glassy carbons and imaging of single pentagonal rings in microporous carbons [4]. Pentagonal rings within a hexagonal network introduce bowl-shaped or Gauss positive curvature, $K > 0$. While fullerene-like graphenes help to resolve many structural features of carbons [4], the positive curvature of fullerenes cannot create three-dimensional (3D) connected networks.

Inspired by Schwartz's study of triply periodic minimal surfaces, Mackay and Terrones proposed 3D carbon networks warped by ≥ 7 -membered rings, providing saddle-shaped or Gauss negative curvature, $K < 0$ [6]. These schwarzite structures are theoretically purely sp^2 , low reactivity nanoforms that form a continuous solid. Layered schwarzites have been computationally explored but the connectivity requires high symmetry [7], contrary to the low-symmetry found in electron microscopy experiments [4]. Another topological element that has found recent experimental [8,9] and theoretical [10] support is Y -shaped or T -shaped junctions which connect graphene fragments via a line defect of sp^3 bonds. Although these junctions create porosity, they require high symmetry and many more sp^3 bonds than are observed experimentally [11]. Despite the evidence for all of these topological textures, it is not obvious how to combine the various structural elements into a coherent 3D model. In this Letter, we address this problem by making use of a suite of recently constructed 3D graphene networks. Using a surface mesh approach, we analyze the topology of the networks and extract the global curvature. This analysis allows us to address two key questions: (i) to what degree does each topology contribute to the curvature? and (ii) how do these textures coexist?

The 3D graphene networks have been previously reported by ourselves, and were generated via self-assembly of carbon atoms using an annealed molecular dynamics methodology [12]. The models span a density range from 0.5 to 1.5 g/cm³. Containing around 32 000

atoms, the structures were large enough to contain all of the topological features described above, including ribbons, micropores, fullerene-like curvature and schwarzitlike curvature. Extensive characterization agreed well with experimental data, such as HRTEM, x-ray, and neutron diffraction scattering, electron energy loss spectroscopy, pore-size distributions, mechanical properties, and thermal conductivity [12–15].

The standard approach to probe the topology of disordered graphene networks uses ring statistics [12,16,17]. An excess of pentagons over heptagons gives a net positive curvature, as in fullerenes, and an excess of heptagons and octagons over pentagons gives negative curvature, as in schwarzites. The rings are related to connectivity according to the well-known Euler-Poincaré polyhedral equation,

$$\sum_{n=3}^{+\infty} (6-n)F_n = 12(1-g). \quad (1)$$

Equation (1) relates the sum of rings or faces, F_n , with cycle count, n , to the genus, g , of the network (genus being a measure of the number of “holes” or “handles” in a surface) [3,18]. For example to connect a periodic carbon schwarzite in 3D, the network must possess at least three holes, $g \geq 3$. This sets the requirement from Eq. (1) for an excess of nonhexagonal rings, F_n , with $n \geq 7$ providing a negatively Gaussian curved network in schwarzites. However, Eq. (1) does not hold for disordered carbon structures as the networks are not purely sp^2 bonded.

Here we use a novel approach that allows us to determine the topology within a disordered carbon network. The first step involves the construction of a triangular mesh from the ring network. In Fig. 1(a) we show one of our graphene networks (0.5 g/cm^3), with an enlarged region in Fig. 1(b) illustrating the mesh construction. The Franzblau algorithm [19] was used to locate rings up to octagons, as larger rings are found to be associated with non- sp^2 vacancies. A vertex is placed at the geometric centre of each ring, V_{ring} and at each atomic site in the rings, V_{sp^2} . These vertices are then joined by edges to the adjacent carbon atoms, E_{sp^2} and to the ring vertices, E_{ring} . This mesh provides a unique surface or graph, $G = \{V_{sp^2}, V_{\text{ring}}, E_{sp^2}, E_{\text{ring}}\}$, as shown in Fig. 1(c). The angular defect, δ , is defined as the difference between the sum of m angles, θ_i , around each vertex $V = \{V_{sp^2}, V_{\text{ring}}\}$, as shown in Fig. 1(b),

$$\delta = 2\pi - \sum_i^m \theta_i. \quad (2)$$

This means that a vertex on a plane has an angular sum of 2π giving $\delta = 0$, while a vertex at a bowl-shaped region has an angular sum less than 2π giving $\delta > 0$ and for saddle-shaped vertices $\delta < 0$. Thus δ gives the sign of the Gaussian curvature for these triangular meshes [20]. The angular

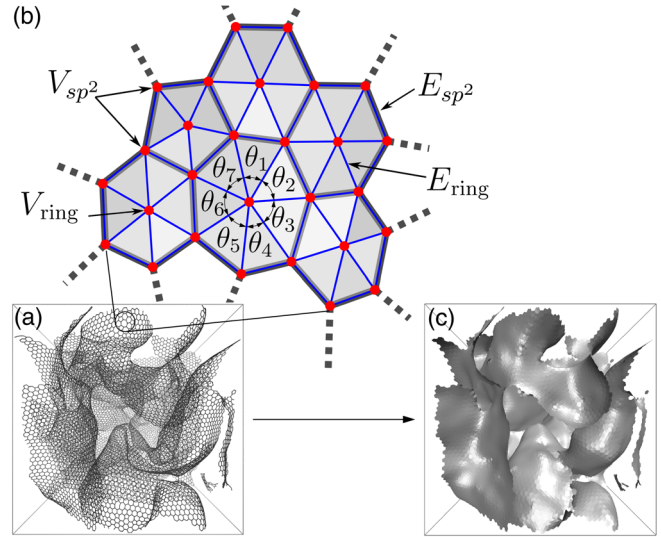


FIG. 1. (a) Periodic disordered carbon network. (b) Enlarged region of the network showing the construction of the triangular mesh: vertices (red dots) are placed on sp^2 atomic sites (V_{sp^2}) and at the centre of each polyaromatic ring (V_{ring}); vertices are connected via edges (blue lines) overlapping atomic bonds (E_{sp^2}) and linking the centre of each ring to its vertices (E_{ring}). The angles around one vertex are shown for the computation of the angular defect. (c) Surface mesh resulting from the procedure.

defect is not computed at vertices at the perimeter or edge (sp -bonded carbons) or tetrahedral carbon atoms (sp^3 -bonded carbons), providing insight into the local curvature of the sp^2 surfaces.

Figure 2 shows a subset of the analyzed networks. At the lowest densities, significant porosity and no stacking of layers is observed, while above 0.9 g/cm^3 stacks of at least three graphene layers appear. Figures 2(a)–2(d) shows nonhexagonal rings colored by cycle number n : blue pentagons, red heptagons, and yellow octagons. These rings form chains known as line dislocations or grain boundaries of alternating pentagons and heptagons, which have been imaged in 2D polycrystalline graphenes [21] and 3D porous carbons [22]. When these dislocations arrange into closed loops with equal numbers of 5- and 7-membered rings they cancel any net global curvature and allow for 2D connectivity. In our networks we have identified both closed and open loops, as observed in Fig. 2(a), with a predominance of open loops and isolated nonhexagonal rings. While the closed loops give rise to planar regions, open loops and isolated nonhexagonal rings are identified in regions of local positive and negative Gaussian curvature. However, as mentioned, counting nonhexagonal rings will not suffice for determining the global curvature in these disordered 3D networks.

Computing the angular defects on each network surface, as shown in Figs. 2(e)–2(h), reveals regions of both saddle-shaped topology in red and bowl-shaped topology in blue.

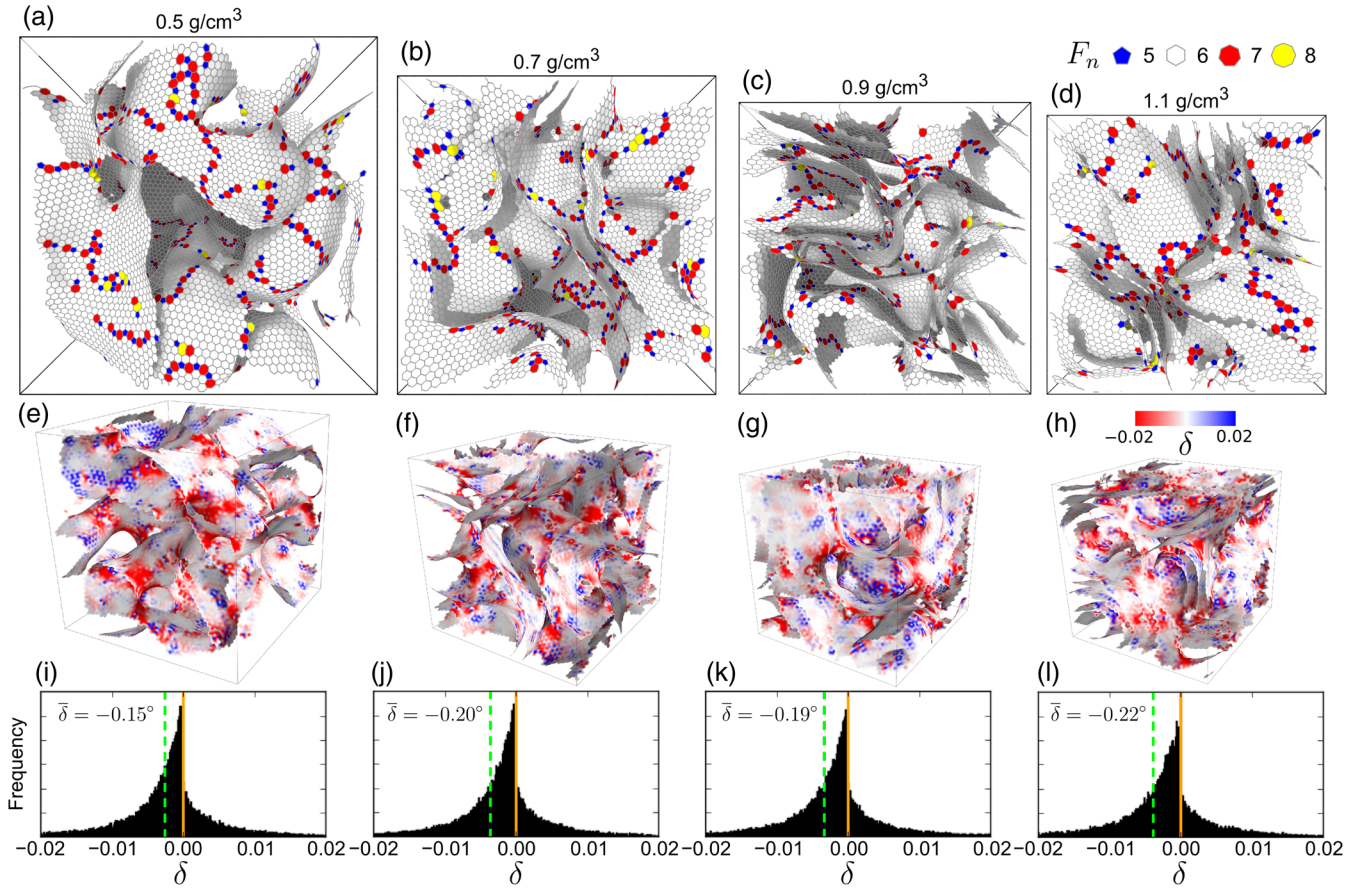


FIG. 2. (a)–(d) Annealed molecular dynamics geometries at densities 0.5, 0.7, 0.9, and 1.1 g/cm³. Pentagonal, heptagonal, and octagonal rings have been colored blue, red, and yellow, respectively. (e)–(h) Angular defect plotted on the mesh. (i)–(l) Histogram of the angular defect with the zero defect (orange line) and average angular defect $\bar{\delta}$ value in degrees (dashed green line).

Visual examination of the structures confirms that the angular defect accurately captures the regions of positive and negative Gaussian curvature. Plotting the histograms of the angular defects, in Figs. 2(i)–2(l), shows a distribution closely centred around $\delta = 0$, which means $K = 0$. However, a clear asymmetry was found in all distributions towards negative curvature, as shown by the average angular defect $\bar{\delta} < 0$. A sensitivity analysis involving ten 8788-atom structures confirms that the results are statistically robust (see the Supplemental Material [23]).

The significance of this net-negative curvature for 3D disordered graphene networks can be further understood in terms of idealized sp^2 carbon nanoforms. For schwarzites the excess negative curvature allows for openings in the networks while continuously connecting in 3D, as given by Eq. (1). In contrast, fullerenes having an excess positive curvature are periodically closed. Ideal graphite, having average curvature of zero, can only possess connectivity in two dimensions. As our networks are predominantly sp^2 (95–97%), therefore approximating ideal carbon nanoforms, we could expect the connectivity to arise from a similar topological argument that net-negative curvature is a requirement for continuous 3D connectivity.

Considering the naming of these networks it would be inappropriate to describe them as purely schwarzitelike due to the presence of positively curved, fullerene-like regions. Recently Schwerdtfeger *et al.* [18] proposed the name G_n -fulleroid to define a high genus net negatively curved closed carbon network containing both 5-membered and ≥ 7 -membered rings, i.e., regions of both positive and negative Gauss curvature (as opposed to a fullerene which contains only 5- and 6-membered rings). As it is inappropriate to ascribe a genus related to the topology due to the presence of edge defects, we suggest these disordered graphene networks have net negative fulleroidlike topology.

While the global curvature of these networks are all similar, the microstructure is very different depending on the density of the network. At low densities, the network consists of single-layer graphene enclosing connected pores, while at high densities randomly oriented stacks of graphene ribbons develop, reducing the porosity of the network to a few isolated voids [12]. Figure 3 shows the computed XRD spectra with the region corresponding to the 002 x-ray reflection highlighted, characteristic of layered graphene [1]. For the highest density network

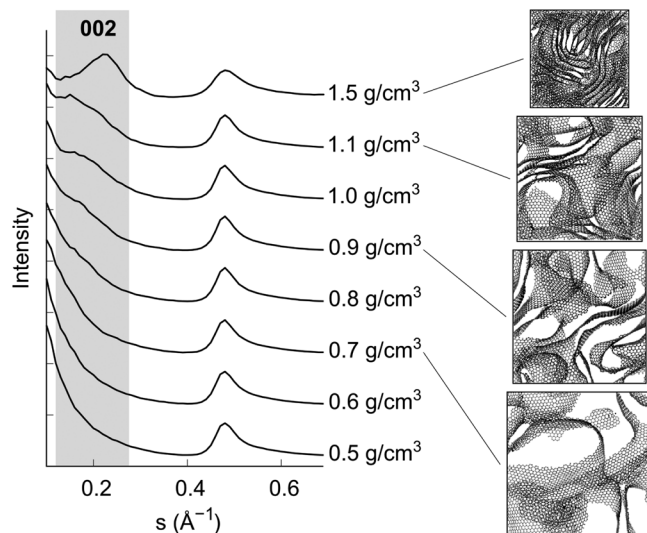


FIG. 3. Computed x-ray diffraction pattern for simulated glassy carbon (top) [14] and porous carbon networks [12,15]. The 002 peak associated with layering is highlighted. The snapshots show a 10 Å slab of the full structures.

prepared at 1.5 g/cm³ this 002 peak is clearly observed [14]. For the porous carbon series the peak starts to develop from 0.9 g/cm³, as a low scattering angle shoulder appears corresponding, by visual inspection, to two or three stacked ribbons.

Further detailed visualization of the bonding networks allows identification of non- sp^2 -bonded atom defects as the key to the coexistence of curved ribbons and stacked layers [see Figs. 4(a)–4(f)]. Table I shows the number of defects as a function of density. Y/T -shaped junctions involve a line of sp^3 defects terminating a graphene sheet perpendicularly to another [see Fig. 4(a)]. These dominate at intermediate densities. Free edges involve sp -bonded atoms terminating a graphene sheet [see Fig. 4(b)(i)]. These defects are found at all densities and vary in length; in the case of the 0.9 g/cc structure the free edges are extensive > 10 rings). Interlayer bonding occurs when two regions of positive Gaussian curvature are bonded via an sp^3 atom [see Fig. 4(b)(ii)]. While these defects are rare, they contribute to the 3D connectivity by linking two regions of positive curvature.

In Figs. 4(c) and 4(d) a screw dislocation defect is highlighted from two different angles. As density increases and layering occurs, these defects become more common. Screw dislocations are free edges wound into a spiral [resembling a $\log(z)$ Riemann surface], well-known in graphite [24,25], anthracite [26] and found in computationally generated 2D pyrocarbon models [27]. These screw dislocations allow the stacked layers to continuously connect and inhibit ideal $ABAB$ (Bernal) stacking. At the highest densities we observe a small number of buckled edges, which form lines of sp -bonded atoms [see Fig. 4(e)].

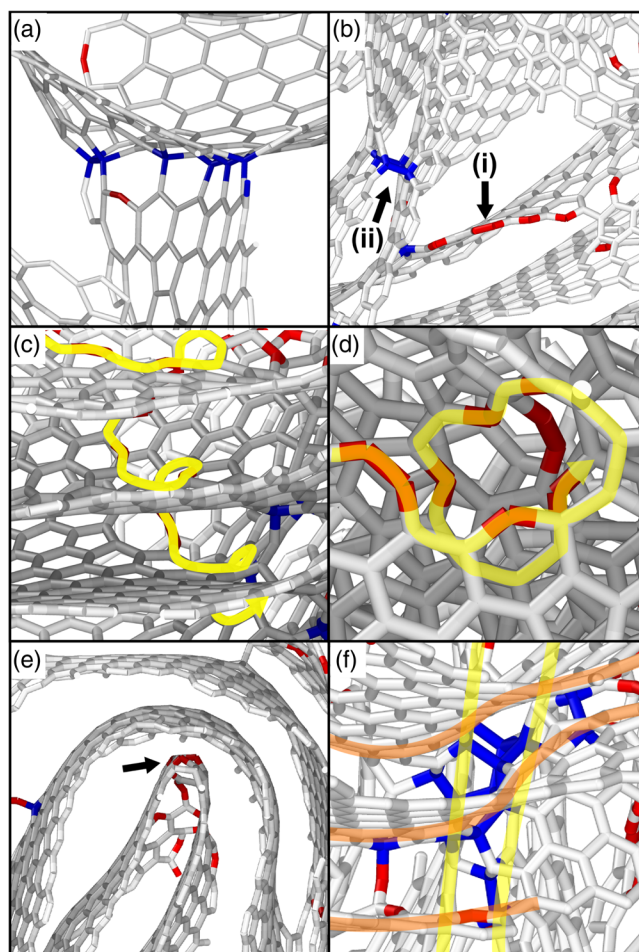


FIG. 4. Slices of the bonding network with sp atoms colored red and sp^3 atoms colored blue. (a) Y/T junction, (b) free edges (i) and interlayer bonding (ii), (c) and (d) a screw dislocation from two different angles, (e) buckled edges and (f) crosshatched ribbons. Yellow and orange highlighting are provided to guide the eye.

These resemble closed edges seen in HRTEM of bilayer graphene [28].

Crosshatching occurs when two ribbons, parallel to each other in one of their axes but perpendicular in the other, form a region of sp^3 bonding, as shown in Fig. 4(f). This common feature in HRTEM imaging of glassy carbon has been proposed theoretically by Balaban [10] but has not been previously achieved in atomistic simulations. The presence of sp^3 bonding in the crosshatching is significant, as traditionally glassy carbon has been used as the purely sp^2 -bonded standard calibration material in electron energy loss spectroscopy (EELS) [11]. Recently, using magic angle corrections in EELS measurements, we found evidence for a small fraction of non- sp^2 -bonded atoms in glassy carbon [11], matching the 5% predicted from our self-assembled carbon model (corresponding to the 1.5 g/cm³ network) [14]. These non- sp^2 defects are critical to resolving the topological complexities arising

TABLE I. Number of non- sp^2 defects as a function of density for the defects shown in Fig. 4.

Density (g/cm ³)	Y/T junction	Free edge	Interlayer	Screw	Buckled	Crosshatched
0.5	4	11	0	0	0	0
0.7	10	16	2	2	0	0
0.9	10	4	0	2	0	1
1.1	6	7	0	6	1	2
1.5	3	6	3	8	2	8

from layering. In particular, the screw dislocations enable the development of layers in these continuously curved disordered graphene networks by avoiding the requirement of high-symmetry in layered schwarzite nanoforms. Based on the carbon science nomenclature [29], we propose that high-density isotropic carbons have a screwed, stacked, net negative fulleroidlike topology.

These results provide insights into the synthesis of porous 3D graphenes. Since layering is linked to density, densities below ≈ 0.9 g/cm³ should be sought to synthesize nanoporous carbons. These low density, negatively curved, foam-like networks are suitable for adsorption applications as the topological features hold open pores and inhibit layering. The regions of positive Gauss curvature are of particular interest as they give rise to reactivity for catalytic applications [30] and a strong flexoelectric charge polarization [31], which we anticipate will significantly effect the adsorption of chemical species such as H₂, CO₂, and CH₄. To synthesize a 3D graphene that maintains the unique electronic properties of planar graphene, such as the Dirac fermion electron dynamics, the number of non- sp^2 defects must also be reduced. This requires that orientable networks must be constructed to allow for the graphene to continuously connect in 3D preventing free edges and Y/T junctions. Such networks can be achieved via templating strategies, as demonstrated by growing graphene on porous sintered metal supports [9,32] and as suggested computationally via zeolite templating [33].

Our analysis also contributes to the ongoing debates on graphitization. In particular, we suggest that the 3D connectivity of these net negative fulleroidlike networks is the origin of their nongraphitizability. Despite containing stacked ribbons, the whole network would not convert to graphite, since significant bond breaking would be required to reduce the connectivity from three to the two dimensions found in a graphitic network. We recently observed such a change in the dimensionality of glassy carbon. Compressing glassy carbon to >35 GPa in a diamond anvil cell at room temperature, we achieved the significant amount of bond breaking necessary to orient the ribbons in 2D and partially graphitize the glassy carbon network. [11].

In conclusion, the analysis of experimentally verified self-assembled nanocarbon models, using a new discrete surface mesh approach, allows for the topology of the

networks to be revealed. These models capture, for the first time, all the experimentally observed topological features in disordered graphene materials from nanoporous through to glassy carbons. We find the structures possess a net negative fulleroidlike topology independent of the microstructural textures present. Densification of the networks gives rise to layered ribbons. Coexistence of stacks of ribbons within a curved graphene network is made topologically possible by a small fraction of non- sp^2 -bonded defects such as screw dislocations.

J. W. M and M. K. acknowledge the financial support from the National Research Foundation (NRF), Prime Minister's Office, Singapore, under its Campus for Research Excellence and Technological Enterprise program and I. S.-M. the fellowship is funded by Australian Research Council (No. FT140100191) as well as helpful discussions on differential topology with Dr Clive Wells, Hughes Hall, Cambridge.

*jwm50@cam.ac.uk

- [1] R. E. Franklin, *Proc. R. Soc.* **209**, 196 (1951).
- [2] G. M. Jenkins and K. Kawamura, *Nature (London)* **231**, 175 (1971).
- [3] S. Gupta and A. Saxena, *MRS Bull.* **39**, 265 (2014).
- [4] P. J. F. Harris, *J. Mater. Sci.* **48**, 565 (2013).
- [5] H. W. Kroto, J. R. Heath, S. C. O'Brien, R. F. Curl, and R. E. Smalley, *Nature (London)* **318**, 162 (1985).
- [6] A. Mackay and H. Terrones, *Nature (London)* **352**, 762 (1991).
- [7] T. C. Petersen, I. K. Snook, I. Yarovsky, D. G. McCulloch, and B. O'Malley, *J. Phys. Chem. C* **111**, 802 (2007).
- [8] H. Badenhorst, *Carbon* **66**, 674 (2014).
- [9] Y. Ito, Y. Tanabe, K. Sugawara, M. Koshino, T. Takahashi, K. Tanigaki, H. Aoki, and M. Chen, *Phys. Chem. Chem. Phys.* **20**, 6024 (2018).
- [10] A. Balaban, D. Klein, and C. Folden, *Chem. Phys. Lett.* **217**, 266 (1994).
- [11] T. B. Shiell, D. G. McCulloch, D. R. McKenzie, M. R. Field, B. Haberl, R. Boehler, B. A. Cook, C. de Tomas, I. Suarez-Martinez, N. A. Marks, and J. E. Bradby, *Phys. Rev. Lett.* **120**, 215701 (2018).
- [12] C. de Tomas, I. Suarez-Martinez, and N. A. Marks, *Appl. Phys. Lett.* **112**, 251907 (2018).
- [13] I. Suarez-Martinez and N. Marks, *Appl. Phys. Lett.* **99**, 033101 (2011).

- [14] C. de Tomas, I. Suarez-Martinez, and N. A. Marks, *Carbon* **109**, 681 (2016).
- [15] C. de Tomas, I. Suarez-Martinez, F. Vallejos-Burgos, M. J. López, K. Kaneko, and N. A. Marks, *Carbon* **119**, 1 (2017).
- [16] M. Thompson, B. Dyatkin, H.-W. Wang, C. Turner, X. Sang, R. Unocic, C. Iacovella, Y. Gogotsi, A. van Duin, and P. Cummings, *C—J. Carbon Res.* **3**, 32 (2017).
- [17] V. L. Deringer, C. Merlet, Y. Hu, T. H. Lee, J. A. Kattirtzi, O. Pecher, G. Csányi, S. R. Elliott, and C. P. Grey, *Chem. Commun. (Cambridge)* **54**, 5988 (2018).
- [18] P. Schwerdtfeger, L. N. Wirz, and J. Avery, *WIREs Comput. Mol. Sci.* **5**, 96 (2015).
- [19] D. S. Franzblau, *Phys. Rev. B* **44**, 4925 (1991).
- [20] V. Borrelli, F. Cazals, and J.-M. Morvan, *Comput. Aided Geom. D* **20**, 319 (2003).
- [21] O. V. Yazyev and Y. P. Chen, *Nat. Nanotechnol.* **9**, 755 (2014).
- [22] J. Guo, J. R. Morris, Y. Ihm, C. I. Contescu, N. C. Gallego, G. Duscher, S. J. Pennycook, and M. F. Chisholm, *Small* **8**, 3283 (2012).
- [23] See Supplemental Material at <http://link.aps.org/supplemental/10.1103/PhysRevLett.123.116105> for the sensitivity analysis on the microstructure and average angular defect.
- [24] G. R. Hennig, *Science* **147**, 733 (1965).
- [25] I. Suarez-Martinez, G. Savini, G. Haffenden, J. M. Campanera, and M. I. Heggie, *Phys. Status Solidi C* **4**, 2958 (2007).
- [26] F. Xu, H. Yu, A. Sadrzadeh, and B. I. Yakobson, *Nano Lett.* **16**, 34 (2016).
- [27] J.-M. Leyssale, J.-P. D. Costa, C. Germain, P. Weisbecker, and G. L. Vignoles, *Carbon* **50**, 4388 (2012).
- [28] Z. Liu, K. Suenaga, P. J. F. Harris, and S. Iijima, *Phys. Rev. Lett.* **102**, 015501 (2009).
- [29] I. Suarez-Martinez, N. Grobert, and C. P. Ewels, *Carbon* **50**, 741 (2012).
- [30] J. W. Martin, G. J. McIntosh, R. Arul, R. N. Oosterbeek, M. Kraft, and T. Söhnle, *Carbon* **125**, 132 (2017).
- [31] J. W. Martin, R. I. Slavchov, E. K. Y. Yapp, J. Akroyd, S. Mosbach, and M. Kraft, *J. Phys. Chem. C* **121**, 27154 (2017).
- [32] H. Nishihara, T. Simura, S. Kobayashi, K. Nomura, R. Berenguer, M. Ito, M. Uchimura, H. Iden, K. Arihara, A. Ohma *et al.*, *Adv. Funct. Mater.* **26**, 6418 (2016).
- [33] E. Braun, Y. Lee, S. M. Moosavi, S. Barthel, R. Mercado, I. A. Baburin, D. M. Proserpio, and B. Smit, *Proc. Natl. Acad. Sci. U.S.A.* **115**, E8116 (2018).